

Holey-structured metamaterial lens for subwavelength resolution in ultrasonic characterization of metallic components

Kiran Kumar Amireddy, Krishnan Balasubramaniam, and Prabhu Rajagopal

Citation: *Appl. Phys. Lett.* **108**, 224101 (2016); doi: 10.1063/1.4950967

View online: <http://dx.doi.org/10.1063/1.4950967>

View Table of Contents: <http://aip.scitation.org/toc/apl/108/22>

Published by the [American Institute of Physics](#)

Holey-structured metamaterial lens for subwavelength resolution in ultrasonic characterization of metallic components

Kiran Kumar Amireddy, Krishnan Balasubramaniam, and Prabhu Rajagopal^{a)}

Centre for Nondestructive Evaluation, Department of Mechanical Engineering, Indian Institute of Technology Madras, Chennai 600036, Tamil Nadu, India

(Received 29 March 2016; accepted 5 May 2016; published online 1 June 2016)

This paper presents the implementation of holey structured metamaterial lens for ultrasonic characterization of subwavelength subsurface defects in metallic components. Experimental results are presented, demonstrating ultrasound-based resolution of side drilled through-holes spaced ($\lambda/5$) in an aluminum block. Numerical simulation is then used to investigate the parameters that can help improve the resolution performance of the metamaterial lens, particularly, the addition of end-conditions. This work has important implications for higher resolution ultrasonic imaging in the context of practical non-destructive imaging and non-invasive material diagnostics. *Published by AIP Publishing.* [<http://dx.doi.org/10.1063/1.4950967>]

Ultrasonic imaging is widely used in non-invasive diagnostics, non-destructive evaluation (NDE), and characterization of materials due to the better attenuation features and reduced risk of radiation effects compared to other techniques.¹ Scattering effects limit the best possible resolution of a given imaging system to half the wavelength of the underlying wave mode or type used.² Imaging resolution below the diffraction limit requires extraction of evanescent waves which carry information about fine features but vanish exponentially in all natural materials away from the source.^{2,3} To amplify the decaying evanescent waves, a hypothetical assumption is that the supporting medium should have a negative refractive index. In the last decade, extensive research has revealed the possibility of overcoming the diffraction limit by using negative indexed media, super-lenses, man-made electromagnetic,⁴⁻⁶ and sonic⁷⁻¹⁰ metamaterial concepts. Such methods have also recently been extended to the acoustic wave regime through various approaches.

Time-reversal techniques,^{11,12} super resolution algorithms,^{13,14} acoustic super-lenses,¹⁵ magnifying acoustic hyper-lenses,¹⁶ phononic crystals,¹⁷⁻²¹ and metamaterials²²⁻²⁶ to amplify evanescent waves have been reported. The main requirement for a negative indexed acoustic medium is that the effective Bulk modulus K and density of material ρ should be simultaneously negative. Such materials do not exist in nature and making them can be expensive: an alternative is to control material parameters through geometry. Corresponding applications for these kinds of materials have shown that they can exceed the diffraction limit in imaging and are easier to manufacture than conventional super-lenses.¹⁵ A deep subwavelength resolution of $\lambda/50$ has been demonstrated by holey structured metamaterials used as a lens for acoustic imaging.²⁷ This is the highest resolution reported in the literature in the sonic regime.

In this paper, we report the implementation of holey structured metamaterials for subwavelength ultrasonic characterization of defects in metals with important implications for NDE

and non-invasive material diagnostics. We consider a practical problem of resolving two circular side-drilled through-holes (SDH) in a metal (aluminum) block. The holes are of 2 mm diameter, with the block dimensions of $100 \times 30 \times 8 \text{ mm}^3$, as illustrated in Figure 1. The two “defects” are separated by a distance of 2.6 mm which is about 0.2 times the wavelength ($\lambda/5$) for compression-wave ultrasonic imaging. Numerical simulation is then used to investigate improvements to the resolution capabilities by controlling the geometry of the metamaterial lens, including the introduction of end conditions.

In the holey structured metamaterial lens, each “hole” acts as a pixel for imaging and improves the resolution by amplifying the decaying evanescent waves through Fabry-Perot resonant modes.⁴ Resonance in turn depends on the geometrical parameters of the metamaterial (diameter, length, and periodicity of the holes) and frequency of excitation as explained below. Consider the wave path in the scenario illustrated in Figure 1(a). Ultrasound scattered by the SDH passes through the meta-lens immersed in water, after which it is picked up by a receiver. Assuming that the scattering acts as a perturbation to the overall plane wave field, for waves passing through the water-filled holey structured lens, we can write

$$(\nabla^2 + k^2)p = 0, \quad (1)$$

where p is the acoustic pressure and k is the wave number. Since the pressure field does not penetrate much into the material, the metamaterial-water interface is assumed rigid²⁸

$$\frac{\partial p}{\partial n} = 0. \quad (2)$$

Solving Equation (1) and writing the expression for transmission coefficient T [see Ref. 27 for further details]

$$T = \frac{4 \left(\frac{d}{\Lambda}\right)^2 Y e^{-ikL}}{1 + Y \left(\left(\frac{d}{\Lambda}\right)^2\right)^2 - \left(\left(1 - Y \left(\left(\frac{d}{\Lambda}\right)^2\right)\right)^2\right) e^{2ikL}}, \quad (3)$$

^{a)} Author to whom correspondence should be addressed. Electronic mail: prajagopal@iitm.ac.in

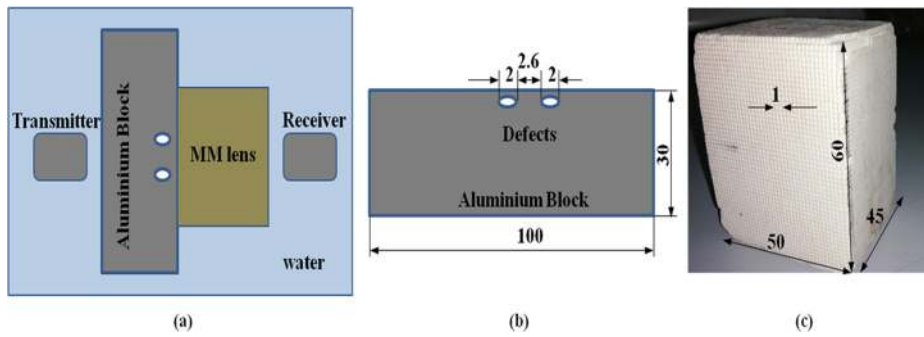


FIG. 1. (a) Illustration of the problem studied for analysis. (b) Cut section of aluminum block with the details of defects presented in it. (c) Photograph of the holey-structured metamaterial lens with dimensions added.

where Y is the ratio of the wavenumber to parallel momentum, d is the diameter, and Λ is the periodicity of the hole array of the meta-lens. If length L of the meta-lens satisfies the following condition, the waves bouncing between the holes experience Fabry-Perot resonance

$$L = \frac{m\lambda}{2n}, \quad (4)$$

where m is an integer, λ is the wavelength of the wave used for imaging, and n is the refractive index.

At the Fabry-Perot resonance condition, the transmission coefficient becomes 1 and hence the meta-lens transfers all the waves (including evanescent waves) from the object plane (input surface) to the image plane (output surface) without any loss.

Figure 1(c) shows the geometry of the holey-structured meta-lens used for the experimentation. The dimensions of the lens were $60 \times 50 \times 45 \text{ mm}^3$, with subwavelength periodic holes of size $d = 1 \text{ mm}$, and a square lattice of period $\Lambda = 2 \text{ mm}$. The meta-lens was made using the selective laser sintering process (obtained from ARCI, Hyderabad, India; see <http://www.arci.res.in/>).

Immersion scan in the through-transmission mode was used in experiments. A commercial 500 kHz central frequency piezoelectric transducer (Panametrics V318, GE measurement & Control) was used for excitation. The excitation is applied as a 3 cycle Hanning windowed tone-burst signal provided through the RITEC 4000 Pulser-Receiver (Ritec Inc., USA). An aluminum block ($100 \times 30 \times 8 \text{ mm}^3$) with two subwavelength side-drilled holes is immersed in water, placed perpendicular to the transducer at a distance of 100 mm in front of it, as shown in Figure 2. Waves scattered from the SDH pass through the lens and are received by

using a Polytec fiberoptic vibrometer (Polytec GmbH, Germany) consisting of an independent OFV-130 optical scanning sensor head and an OFV-551 controller. The output from the controller is fed to a computer through an Agilent DSO 7012B digital storage oscilloscope. A thin retro-reflective tape was attached on the surface of the immersion tank at the spot illuminated by the laser point so as to enhance the optical back-scattering from the laser beam. This fiber optic head was translated across the immersion tank through a National Instruments PCI 7330 (NI Inc., USA) motion controller to receive the signals at a regular intervals of 0.5 mm to complete a B-scan (line scan).

After performing the line scan, the maximum amplitude is obtained from each A-scan (on time trace) and plotted against receiving position, as shown in Figure 3. (Simulation results mentioned in Figure 3 are explained later in this paper.) The grey-colored rectangular boxes indicate the real or actual position of the defects (2 mm holes separated by a distance of 2.6 mm which is about $\lambda/5$ for a frequency of 500 kHz) present in the aluminum block. We find that at the exact defect locations, the signal transmitted by the metamaterial lens shows a strong decrease in amplitude. The positional distance between the amplitude minima in the experimental result is very close to the actual value in the sample. The results demonstrate that the holey-structured metamaterial lens helps to effectively resolve subwavelength ($\lambda/5$) spaced holes in the aluminum block in the ultrasonic regime.

In order to demonstrate the practical attraction and ease of use of this approach, a meta-lens was also constructed by making use of plastic straw tubes sourced off-the-shelf, of size 2 mm in diameter and 60 mm in length as shown in Figure 4(a). This meta-lens was used for subwavelength ultrasonic imaging of two rectangular holes of width 2 mm, separated by 3 mm (which is $\lambda/5$ for a central frequency of 100 kHz in water media) in a thin sheet of paper as illustrated in Figure 4(c).

The maximum amplitude variation is plotted against receiver positions, as shown in Figure 5. As above, the actual defect locations are indicated by grey colored rectangular boxes in the plots, and we observe effective defect resolution with the help of the meta-lens.

For electromagnetic waves¹⁵ and acoustic waves,³ it has been shown that for effective resolution, the periodicity of the array of the holes in the metamaterial lens should be much smaller than the wavelength of the wave used for the imaging.^{3,20} With the help of a commercially available finite element (FE) package,²⁹ we conducted further studies to show

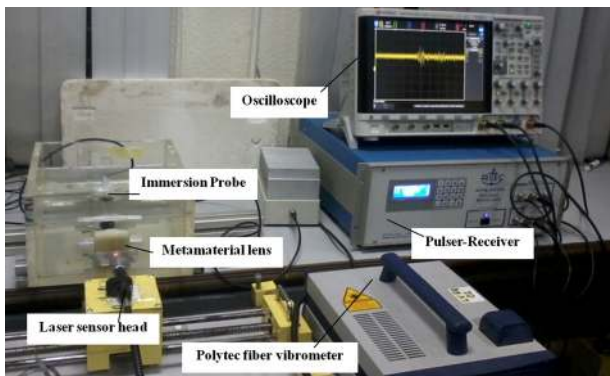


FIG. 2. Photograph of the experimental setup.

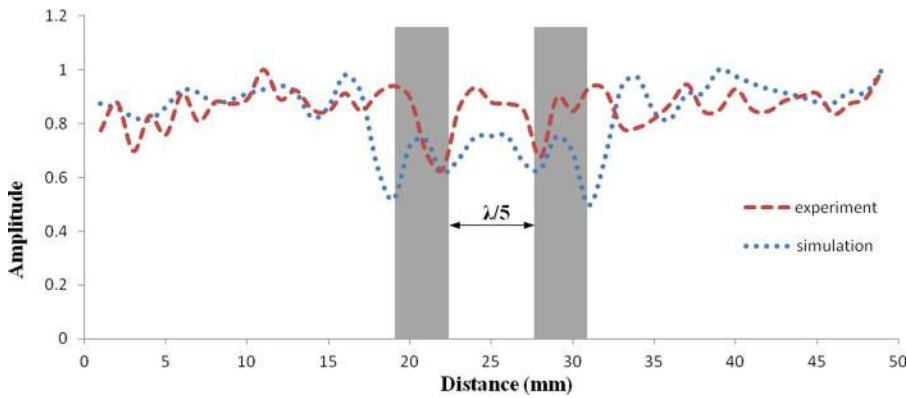


FIG. 3. Experimental and simulated results for normalized amplitude variation with the measurement position across the sample. The two rectangular boxes represent the position of the two subwavelength ($\lambda/5$) spaced defects in the aluminum block.

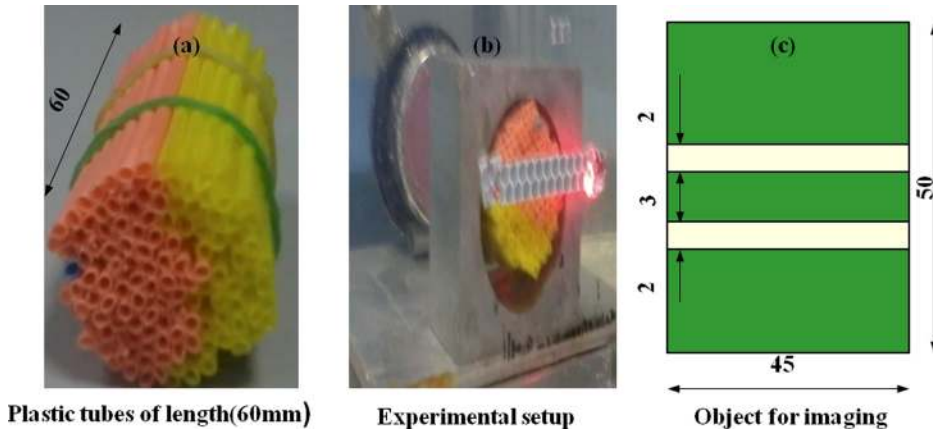


FIG. 4. (a) Photograph of the meta-lens constructed with plastic straw tubes; (b) experimental setup; and (c) illustration of subwavelength spaced holes in a paper of thickness 5 mm.

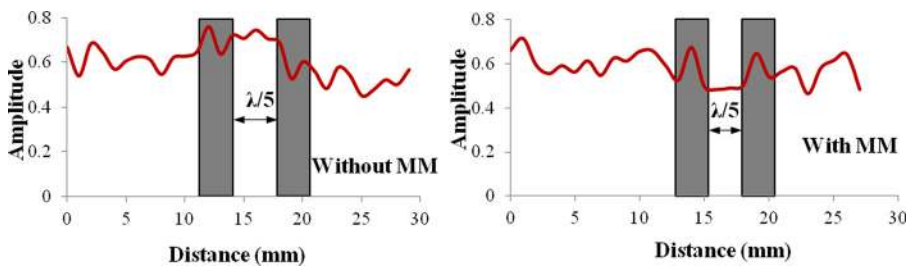


FIG. 5. Experimental results for normalized amplitude variation with the measurement position across the sample with and without the plastic straw tube assembly meta-lens. The two rectangular boxes represent the position of the two subwavelength ($\lambda/5$) spaced defects in a thin sheet of paper.

that the resolution of the meta-lens is improved for smaller hole diameter (0.5 mm) and period (1 mm). A 2-D FE model was created with dimensions $200 \times 110 \text{ mm}^2$, chosen to avoid reflections from the model boundaries. The overall model consists of one part each for the defective sample and the metamaterial immersed in water, respectively, as shown in

Figure 6. For both parts, 4-noded quadrilateral mesh with a seed size of 0.15 mm (which is about $\lambda/20$ for 500 kHz in water for mesh convergence³⁰) was used. For the model of the defective sample, mechanical properties of aluminum were assigned, with Young's modulus $E = 69 \text{ GPa}$, density $\rho = 2700 \text{ kg/m}^3$, and Poisson's ratio $\nu = 0.334$. For simulating

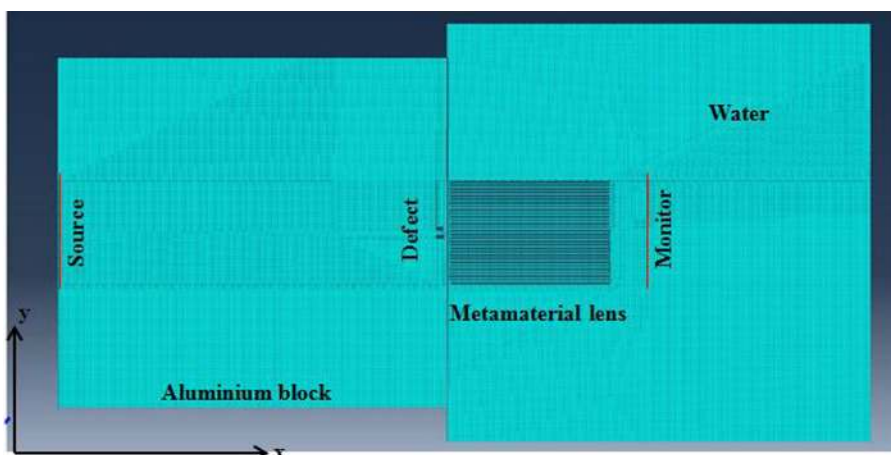


FIG. 6. Snapshot of FE model with mesh.

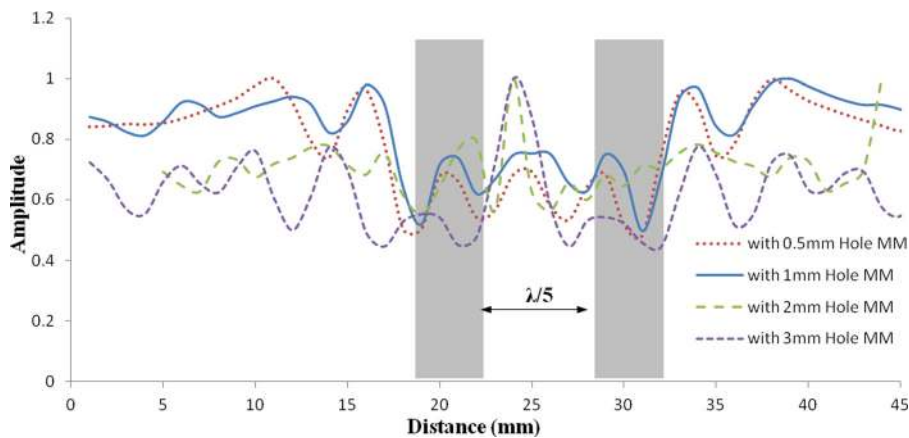


FIG. 7. Simulated results of normalized amplitude variation with the measurement position across the sample, for different hole diameter values. The two rectangular boxes represent the position of the two subwavelength ($\lambda/5$) spaced defects in the aluminum block.

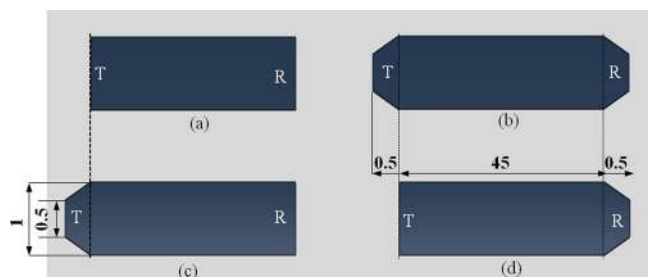


FIG. 8. Different kinds of end conditions imparted to the meta-lens for performance analysis (T is transmitter and R is receiver) (a) without end conditions, (b) both sided end conditions, (c) transmitter side end conditions, and (d) receiver side end conditions.

a line scan across the metamaterial immersed in water, a 2-D model of size $240 \times 120 \text{ mm}^2$ was created and assigned water (acoustic medium) properties, with density $\rho = 1000 \text{ kg/m}^3$ and Bulk modulus $K = 2.2 \text{ GPa}$. A 2-D holey structured metamaterial of length 45 mm with a hole thickness of 1 mm and a periodicity of 2 mm is realized by setting rigid (pressure is zero) boundary conditions on selected nodal lines.

The two parts were so created as to have a common boundary and during assembly a tie constraint is given at the interface to allow for the wave propagation from aluminium sample into the metamaterial. Waves are generated in the model by exciting the left boundary of the aluminium sample in the “x” direction with nodal forces consisting of 3 cycle Hanning windowed tone burst signals centered at 500 kHz. Ultrasonic wave propagation in the sample is then simulated using the explicit FE algorithm provided in the commercial package.²⁹ Analysis was run for a total time

period of $90 \mu\text{s}$ which is sufficient for longitudinal waves to reach the right end of the whole model. Nodes along a vertical line at a fixed distance from the meta-lens were chosen for monitoring the waves scattered by the circular hole defects in the aluminium sample and transmitted by the meta-lens. The variation of the maximum amplitude obtained from the A-scans with the monitored position is shown together with experimental results presented earlier, in Figure 3. Experimental results agree well with the numerical prediction, thus giving confidence in this simulation approach, and our numerical model. By making use of this model, we showed that the resolution of the meta-lens can be improved by a smaller array of holes with less periodicity: for example, the variation of resolution with meta-lens hole diameter is shown in Figure 7.

Using the same numerical simulation approach and models, we also argue that the resolution of the meta-lens is greatly improved by imparting suitable end conditions. We considered the following four cases for analysis: (i) without end conditions (WOEC), (ii) both sided end conditions (BSEC), (iii) transmitter side end conditions (TSEC), and (iv) receiver side end conditions (RSEC). In all cases, the end-condition consisted of a simple linear taper resulting in a reduction in hole size of 0.5 mm (starting with 1 mm), as shown in Figure 8.

Figure 9 presents the resolution plots for these four types of proposed end conditions. Ultrasonic transmission through the BSEC lens and WOEC lens was not effective (due to low impedance mismatch at the ends), hence the resolution is poor with these types of meta-lenses. With TSEC, the resolution is moderate because all waves scattered from the defects

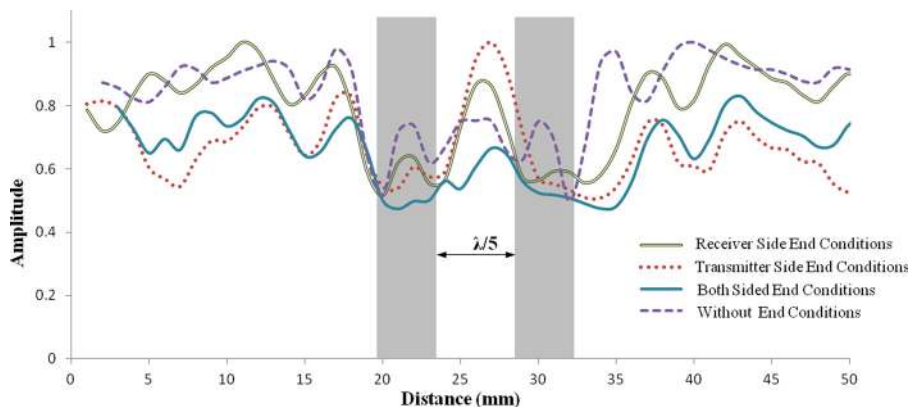


FIG. 9. Simulated results of normalized amplitude variation with monitoring position, for different end conditions imparted to the holey structured metamaterial lens.

in the sample may not pass through the meta-lens due to reduced entrance size. In case of RSEC, waves can effectively couple into the meta-lens because of un-constricted entrance into the holes. The narrowing of the exit holes seems to focus the waves in addition to the Fabry-Perot resonances, yielding improved higher resolution. Authors are currently investigating the physics enabling the improvement in resolution with RSEC, and also aspects such as the influence of taper slope and geometry (instead of a simple linear form as assumed here).

This paper demonstrated the application of hole-structured metamaterial lens for subwavelength imaging in the context of ultrasonic NDE. The meta-lens improves resolution down to the sub-wavelength regime through Fabry-Perot resonance phenomenon. An advantage of this approach is that the resonant frequency can be changed by modifying the diameter of the hole, length of the meta-lens, and periodicity. Thus, although we have demonstrated a resolution of $\lambda/5$ here, a higher resolution can be achieved by creating metamaterials with finer hole diameter, and this is a matter for further work at the authors' research group at this time. Experimental results also demonstrate that the proposed lens is easily fabricated, with the possibility of being made from cheaply available tubes and is capable of resolving defects separated at a distance below the diffraction limit. A numerical model has been developed to evaluate the transmission property of evanescent waves through the hole-structured metamaterial. Simulations show that imparting end conditions at receiver side (RSEC) can improve the resolution provided by a given meta-lens. Further work by the authors is also examining the physics of the end-condition based improvement in resolution and amplification of evanescent waves.

Authors gratefully acknowledge helpful discussions with Dr. Balaji Srinivasan, Associate Professor, Electrical Engineering Department, Indian Institute of Technology-Madras, Chennai, T.N., India.

- ¹W. S. Gan, *Acoustical Imaging: Techniques and Applications for Engineers* (John Wiley & Sons, Ltd., Chichester, UK, 2012), pp. 5–13.
- ²X. Zhang and Z. Liu, *Nat. Mater.* **7**(6), 435–441 (2008).
- ³Y. Cheng, C. Zhou, Q. Wei, D. Wu, and X. Liu, *Appl. Phys. Lett.* **103**(22), 224104 (2013).
- ⁴V. G. Veselago, *Sov. Phys. Usp.* **10**(4), 509–514 (1968).
- ⁵D. R. Smith, W. J. Padilla, D. C. Vier, S. C. Nemat-Nasser, and S. Schultz, *Phys. Rev. Lett.* **84**, 4184–4187 (2000).
- ⁶V. M. Shalaev, *Nat. Photonics* **1**, 41–48 (2007).
- ⁷Z. Liu, X. Zhang, Y. Mao, Y. Y. Zhu, Z. Yang, C. T. Chan, and P. Sheng, *Science* **289**, 1734–1736 (2000).
- ⁸N. Fang, D. Xi, J. Xu, M. Ambati, W. Srituravanich, C. Sun, and X. Zhang, *Nat. Mater.* **5**, 452–456 (2006).
- ⁹S. Zhang, L. Yin, and N. Fang, *Phys. Rev. Lett.* **102**, 194301 (2009).
- ¹⁰S. A. Cummer, J. Christensen, and A. Alu, *Nat. Rev. Mater.* **1**, 16001 (2016).
- ¹¹J. de Rosny and M. Fink, *Phys. Rev. Lett.* **89**, 124301 (2002).
- ¹²G. Lerosey, J. de Rosny, A. Tourin, and M. Fink, *Science* **315**, 1120–1122 (2007).
- ¹³F. Simonetti, *Phys. Rev. E* **73**, 036619 (2006).
- ¹⁴F. Simonetti, L. Huang, and N. Duric, *J. Appl. Phys.* **101**, 083103 (2007).
- ¹⁵Z. Liu, S. Durant, H. Lee, Y. Pikus, N. Fang, Y. Xiong, C. Sun, and X. Zhang, *Nano Lett.* **7**, 403–408 (2007).
- ¹⁶D. Liu and Z. Liu, *Nat. Commun.* **3**, 1205 (2012).
- ¹⁷S. Yang, J. H. Page, Z. Liu, M. L. Cowan, C. T. Chan, and P. Sheng, *Phys. Rev. Lett.* **93**, 024301 (2004).
- ¹⁸X. D. Zhang and Z. Y. Liu, *Appl. Phys. Lett.* **85**, 341 (2004).
- ¹⁹A. Sukhovich, L. Jing, and J. H. Page, *Phys. Rev. B* **77**, 014301 (2008).
- ²⁰A. Sukhovich, B. Merheb, K. Muralidharan, J. O. Vasseur, Y. Pennec, P. A. Deymier, and J. H. Page, *Phys. Rev. Lett.* **102**, 154301 (2009).
- ²¹Z. He, F. Cai, Y. Ding, and Z. Liu, *Appl. Phys. Lett.* **93**, 233503 (2008).
- ²²M. Ke, Z. Liu, Z. Cheng, J. Li, P. Peng, and J. Shi, *Solid State Commun.* **142**, 177–180 (2007).
- ²³C. M. Soukoulis, S. Linden, and M. Wegener, *Science* **315**, 47–49 (2007).
- ²⁴N. Fang, H. Lee, C. Sun, and X. Zhang, *Science* **308**, 534–537 (2005).
- ²⁵T. Taubner, D. Korobkin, Y. Urzhumov, G. Shvets, and R. Hillenbrand, *Science* **313**, 1595 (2006).
- ²⁶Z. Liu, H. Lee, Y. Xiong, C. Sun, and X. Zhang, *Science* **315**, 1686 (2007).
- ²⁷J. Zhu, J. Christensen, J. Jung, L. Martin-Moreno, X. Yin, L. Fok, X. Zhang, and F. J. Garcia-Vidal, *Nat. Phys.* **7**(1), 52–55 (2011).
- ²⁸H. Estrada and F. Meseguer, in Proceedings of ICSV16, Krakow, Poland, 5–9 July 2009.
- ²⁹See <http://www.3ds.com/products/simulia/portfolio/abaqus/abaqus-portfolio> for ABAQUS. Analysis User's Manual. Version 6.10-1; accessed 28 July 2015.
- ³⁰A. Ramdhas, R. K. Pattanayak, K. Balasubramaniam, and P. Rajagopal, *Ultrasonics* **56**, 232–242 (2015).